PNAS RESEARCH ARTICLE | ENVIRONMENTAL SCIENCES
EARTH, ATMOSPHERIC, AND PLANETARY SCIENCES

Pervasive alterations to snow-dominated ecosystem functions under climate change

William R. Wieder[a,b,1], Daniel Kennedy[a], Flavio Lehner[c,a], Keith N. Musselman[b], Keith B. Rodgers[d,e], Nan Rosenbloom[a], Isla R. Simpson[a], and Ryohei Yamaguchi[d,e,2]

Edited by Dennis Hartmann, University of Washington, Seattle, WA; received February 9, 2022; accepted April 28, 2022

Climate change projections consistently demonstrate that warming temperatures and dwindling seasonal snowpack will elicit cascading effects on ecosystem function and water resource availability. Despite this consensus, little is known about potential changes in the variability of ecohydrological conditions, which is also required to inform climate change adaptation and mitigation strategies. Considering potential changes in ecohydrological variability is critical to evaluating the emergence of trends, assessing the likelihood of extreme events such as floods and droughts, and identifying when tipping points may be reached that fundamentally alter ecohydrological function. Using a single-model Large Ensemble with sophisticated terrestrial ecosystem representation, we characterize projected changes in the mean state and variability of ecohydrological processes in historically snow-dominated regions of the Northern Hemisphere. Widespread snowpack reductions, earlier snowmelt timing, longer growing seasons, drier soils, and increased fire risk are projected for this century under a high-emissions scenario. In addition to these changes in the mean state, increased variability in winter snowmelt will increase growing-season water deficits and increase the stochasticity of runoff. Thus, with warming, declining snowpack loses its dependable buffering capacity so that runoff quantity and timing more closely reflect the episodic characteristics of precipitation. This results in a declining predictability of annual runoff from maximum snow water equivalent, which has critical implications for ecosystem stress and water resource management. Our results suggest that there is a strong likelihood of pervasive alterations to ecohydrological function that may be expected with climate change.

climate change | ecohydrology | water resources | internal variability | large ensemble

Significance

Climate change will alter the mean ecohydrological state, but little is known about potential changes in ecohydrological variability that are required to inform climate change adaptation and mitigation strategies. Our results demonstrate pervasive alterations to the variability of water fluxes, water storage, and disturbance by the end of this century. Projected warming will reduce winter snow accumulation and increase the fraction of snow that melts during winter, blurring the seasonal distinction between periods of winter snow accumulation and its subsequent melt in the spring and summer. Notably, we find that in the future, runoff quantity and timing will be less predictable from snow, more closely reflecting the stochastic character of precipitation—findings that have critical implications for water resource management.

Seasonal snowmelt provides freshwater resources that sustain ecosystems, agriculture, recreation, and livelihoods. Under climate change scenarios, snowpack in the Northern Hemisphere is projected to decline through the end of this century (1), raising concerns about future water security and ecosystem function (2, 3). Terrestrial and freshwater ecosystems in snow-dominated regions depend on the reliable accumulation of snow during the winter and its subsequent melt in the spring and summer to regulate water availability, phenology, productivity, and streamflow. The storage and predictable release of snowmelt are also critical for water-management systems. Shifts in the timing of winter snowmelt and declining runoff efficiency may reduce the predictability of streamflow and drought under climate change scenarios (4, 5). Changes in the timing of snowmelt and runoff that have been projected for decades are now being observed across much of western North America (6, 7), suggesting that anthropogenic activity is already altering continental-scale ecohydrological function.

Changes in the ecosystems that provide freshwater resources will be determined by physical changes in the climate system, plant physiological responses to elevated CO_2, alteration of disturbance regimes, and their interactions (8–10). The interaction between climate change and plant physiological response has important implications for carbon and water fluxes under future scenarios. For example, in terrestrial ecosystems with consistent seasonal snowpack, the timing of spring melt is strongly correlated with plant phenological events like leaf emergence and flowering (11–13). While it is generally accepted that warmer temperatures and earlier spring snowmelt extend the length of the growing season, which can increase productivity and the strength of the carbon sink in Northern Hemisphere ecosystems (14–16), there is evidence of substantial heterogeneity of this response in cold regions (17). Earlier snowmelt and longer growing seasons may cause growing-season soil-water deficits that can reduce productivity and increase wildfire risk (18–21). Moreover, phenological changes associated with earlier snowmelt potentially disrupt ecological interactions that can lead to shifts in community composition and function (22, 23). Thus, changes in the timing and magnitude of snowmelt can have cascading influences on terrestrial ecosystems, freshwater resources, and their potential interactions.

Author contributions: W.R.W. designed research; W.R.W. performed research; W.R.W. and D.K. contributed new reagents/analytic tools; W.R.W. and K.N.M. analyzed data; K.R. contributed to the design the CESM2-LE simulations; N.R. set up and coordinated the CESM2-LE simulations; and W.R.W., D.K., F.L., K.N.M., K.B.R., N.R., I.R.S., and R.Y. wrote the paper.

The authors declare no competing interest.

This article is a PNAS Direct Submission.

[1]To whom correspondence may be addressed. Email: wwieder@ucar.edu.

[2]Present address: Research Institute for Global Change, Japan Agency for Marine-Earth Science and Technology, Kanagawa, Japan.

This article contains supporting information online at http://www.pnas.org/lookup/suppl/doi:10.1073/pnas.2202393119/-/DCSupplemental.

Published July 18, 2022.

Climate variability in snow-dominated ecosystems complicates the detection and attribution of forced trends (6, 11). Furthermore, understanding potential changes in climate variability will be critical for successful adaptation and mitigation strategies (24–26). Considering potential changes in variability is critical to evaluating the emergence of trends, assessing the likelihood of extreme events, and identifying when tipping points may be reached that fundamentally alter ecohydrological function (27–29). Large Ensemble (LE) climate model simulations provide a powerful means to evaluate both forced changes in variance and forced changes in the seasonal cycle (30–32). With enhanced complexity in their land components, these models can also facilitate mechanistic understanding of changes in terrestrial ecosystems related to biogeochemical cycles or hydrological processes (33–36). Beyond mean state changes, ecosystems in snow-dominated regions may be highly sensitive to changes in variability, but limited model ensemble size, resolution, and complexity have, so far, precluded this examination. Here, we utilize a state-of-the-art LE to investigate how changes in the mean state and internal variability of snow accumulation and melt may impact the ecohydrology and biogeochemistry of historically snow-dominated ecosystems.

Results and Discussion

Historical Results. We characterize changes in the mean state and variability of land processes under a historical/SSP3-7.0 pathway. Our analysis uses the Community Earth System Model, version 2, Large Ensemble (CESM2-LE; *Materials and Methods*) (26), because of its combination of ensemble size, spatial resolution, land model complexity, and the requisite high-frequency output. To characterize the forced response from climate change, we compare a variety of quantities that describe snow–hydrology–ecosystem relations between a future scenario (2070 to 2099) and a historical baseline (1940 to 1969) using 40 CESM2-LE members.

In historically snow-dominated regions, defined here as grid-cells with >30 mm snow water equivalent (SWE) for >3 mo (*Materials and Methods*), the CESM2-LE adequately simulates the mean climatology of historical temperature and precipitation, although regional biases in the model exist (Fig. 1 and *SI Appendix*, Fig. S1). An exhaustive evaluation of CESM2 strengths and deficiencies is outside the scope of this study (instead see refs. 26, 37–41), but a comparison of the model mean state with observational benchmarks illustrates that the CESM2-LE simulates high SWE biases (+46 mm H_2O across the domain) (*SI Appendix*, Fig. S1) (42). This high SWE bias occurs despite also having a warm winter temperature bias (+3 K) and low winter precipitation bias (-0.02 mm d^{-1}). High SWE biases could reflect an underestimation of ablation rates in the model, additional model structural uncertainties, uncertainties in global SWE reconstructions, and/or inconsistencies among observationally derived benchmarks (43). These biases in the model's mean state, however, may not be a good metric by which to evaluate the model skill at representing trends in snow accumulation and melt, often referred to in hydrology as the climate sensitivity of snow.

The magnitude of SWE trends simulated by the CESM2-LE is reasonable compared with estimates from global reanalysis over the historical record (1), with the observationally derived dataset generally falling within the 40-member ensemble range over the entire domain (*SI Appendix*, Fig. S2). We note that reconstructions of SWE and snow depth are difficult to make and highly uncertain, especially at global scales (44, 45). Observationally derived snow data products that assimilate in situ station data with statistical models and gridded climate reanalysis provide high-quality estimates of regional SWE totals and trends (46–48). Here, we interchangeably use the terms *observed* and *observationally derived* to refer to these gridded snow products. Comparing the CESM2-LE mean state and trends with the University of Arizona SWE dataset (46, 49) over the conterminous United States again suggests that the CESM2-LE has a high SWE bias (50) (*SI Appendix*, Fig. S3). The CESM2-LE mean also shows declining maximum SWE trends over the historical record, which is consistent with the observational estimates in parts of the western United States but not in the upper Midwest or Northeast, with observational trends falling outside the 40-member ensemble range in these regions. The observationally derived trends in maximum SWE are generally driven by winter warming over the western United States and increases in precipitation over the eastern United States (50). The 40-member CESM2-LE mean broadly captures the appropriate global trajectories of observed climate trends (1970 to 2020), but it also simulates rates of regional winter warming, particularly across the eastern United States, that are higher than observational estimates (*SI Appendix*, Fig. S4). This high winter-warming bias overwhelms winter precipitation changes in the eastern United States and reverses the sign of SWE trends over the region in the CESM2-LE compared with observations.

Projected Changes in the Mean State. Under the SSP3-7.0 climate change scenario, terrestrial ecosystems experience higher precipitation rates and warmer temperatures with climate change (Fig. 1). Precipitation increases are most notable in regions with maritime climates (*SI Appendix*, Fig. S5*A*). Warmer temperatures result in thinner snowpack and reductions in SWE by the end of the century. Snow accumulates later in the fall and melts earlier in the spring, resulting in a longer growing season, compared with the historical baseline (Fig. 1). With a longer growing season, characterized by an earlier spring green-up and later fall senescence, ecosystems maintain higher gross primary productivity (GPP) (14, 26).

Widespread shifts in water fluxes, water storage, and disturbance such as wildfire are projected to occur this century. Compared with the historical baseline, earlier snowmelt shifts the seasonal timing of runoff, causing runoff to exhibit higher and more episodic winter flow, earlier spring peaks, and reduced summer volumes (Fig. 1*E*) but no changes in annual discharge (discussed in Declining Predictability of Freshwater Ecosystems and Water Resources). The earlier melt and reduced snowpack result in drier soil-moisture conditions during the growing season (Fig. 1*F*). Amplifications of carbon fluxes through increased plant productivity (Fig. 1*D*) in the CESM2-LE are achieved with only modest increases in terrestrial evapotranspiration (ET; Fig. 1*G*). Together, these results imply a significant increase in the ecosystem water-use efficiency that is simulated in the CESM2-LE (40). Finally, drier soils and reduced relative humidity increase average fire counts more than threefold across the domain by the end of this century, especially during the warmest, driest months (Fig. 1*H*). These changes, however, are not distributed evenly across the domain.

The relatively modest changes in runoff and ET (Fig. 1 *E* and *G*) mask the spatial variability in future projections (Fig. 2 and *SI Appendix*, Fig. S5). Ensemble mean annual ET fluxes increase across large regions of Arctic tundra, boreal forests, and the North American Rocky Mountains. Increases in annual ET are driven by longer growing seasons and warmer temperatures, which are broadly consistent with observed greening over high-latitude ecosystems (14–16, 51, 52). Recent work, however, raises concerns about the limits of these ecosystems to maintain sustained increases in productivity under climate change (17). For example, observations suggest that earlier spring green-up events deplete soil-water resources, resulting in anomalously

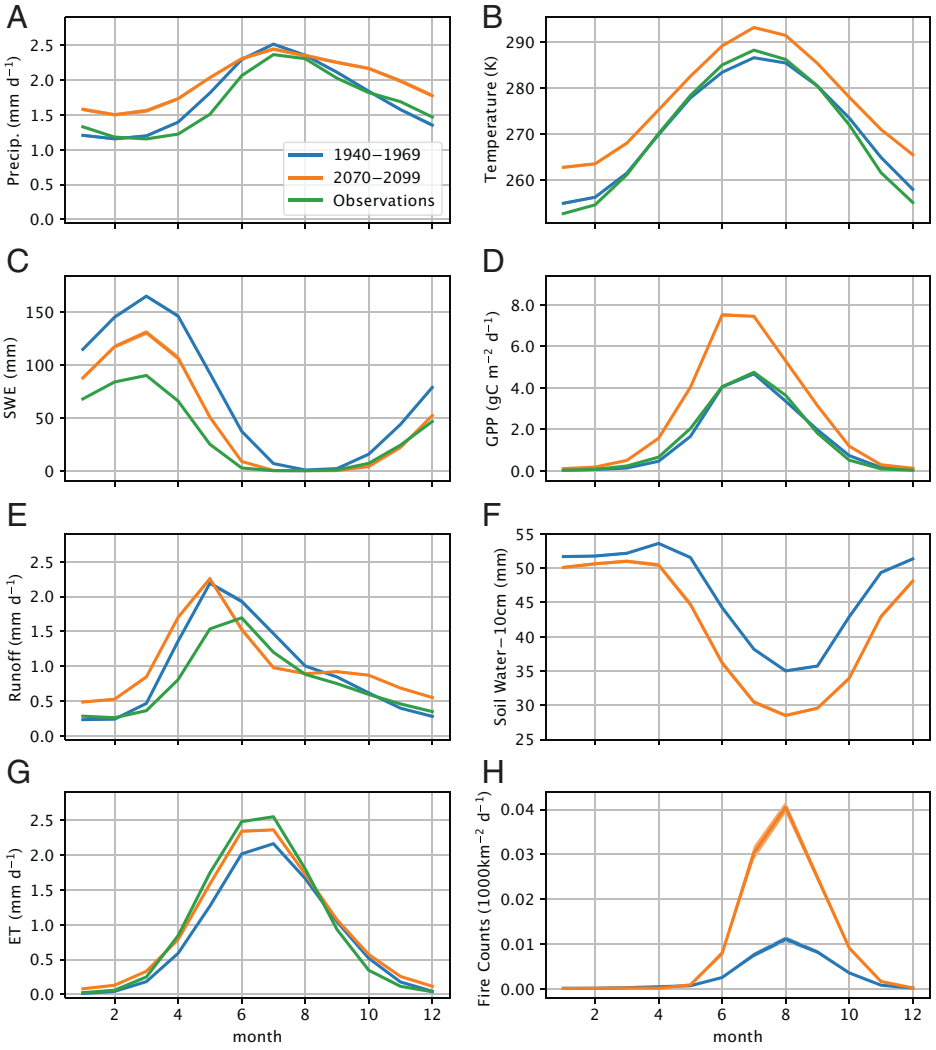

Fig. 1. Climate-driven shifts in the seasonal cycle of ecohydrological processes. The mean seasonal climatology over vegetated gridcells of historically snow-dominated regions showing (*A*) precipitation; (*B*) air temperature; (*C*) SWE; (*D*) GPP; (*E*) runoff; (*F*) soil water, 10-cm depth; (*G*) ET; and (*H*) fire counts. Lines show the monthly mean (± 1 SD) from 40 members of the CESM2-LE over the baseline period (1940 to 1969; blue lines) and future scenario (2070 to 2099; orange lines). The observational climatology for select variables over the domain are also provided (green lines) Note, by focusing on the forced response and taking statistics over the entire domain, the ensemble SD is very small. The domain of historically snow-dominated regions is defined in the Northern Hemisphere to be where the ensemble mean monthly SWE over the initial years of the simulation (1850 to 1880) was greater than 30 mm for at least 3 mo of each year, and where gridcells that were initially snow covered for 12 mo were excluded. Precip, precipitation.

low productivity in subsequent summer and fall seasons (19, 53). CESM2 qualitatively captures this response over the historical period (54), but the strength of this feedback has not been well quantified in future scenarios. Under climate change, many terrestrial ecosystems in the CESM2-LE show increases in productivity and the partitioning of precipitation to ET ("green water"), which reduces surface-water availability in soil moisture and runoff ("brown water" and "blue water" resources, respectively (35) (Fig. 2 *B* and *C* and *SI Appendix*, Fig. S5*B*). Notable exceptions, where large increases in precipitation increase the annual runoff fraction and maintain summer soil-water content, include East Asia, the Himalayas, and northwestern North America.

Finally, the number of fire counts estimated in the CESM2-LE increases dramatically under the SSP3-7.0 scenario. The largest increase in fire counts occurs across the midlatitudes (Fig. 2*D*), whereas the largest proportional increase in fire counts occurs in northeastern North America and Europe, which historically had very low fire counts (*SI Appendix*, Fig. S5*D*). We also note that fire modeling poses a number of known important challenges in Earth system modeling (55), and the CLM5 model used in the CESM2-LE is not exempt from these challenges. For example, the CESM2-LE shows relatively little change in the absolute or relative number of fire counts that are simulated across high-latitude regions of North America and Asia, in apparent contradiction with large fire disturbances that are observed across high-latitude ecosystems (56). Indeed, uncertainties in the impacts of future fire risk on climate, ecosystems, air quality, and livelihoods underscore the importance of improving the representation of disturbances like fire in Earth system models.

Changing Variability of Snow Accumulation and Melt. To explore the projected changes in the mean state and variability of snow accumulation and melt, we focus on an individual gridcell in the northern US Rocky Mountains where snow-water resources are carefully monitored to support critical hydropower and agricultural industries (Fig. 3 and *SI Appendix*, Fig. S6). An equivalent analysis for a gridcell in the central US Rocky Mountains leads to similar conclusions (*SI Appendix*, Fig. S7). In Fig. 3, the ensemble mean shows a steady decline in maximum SWE starting around the year 2000 and reduces by nearly a factor of 4 by 2100 under

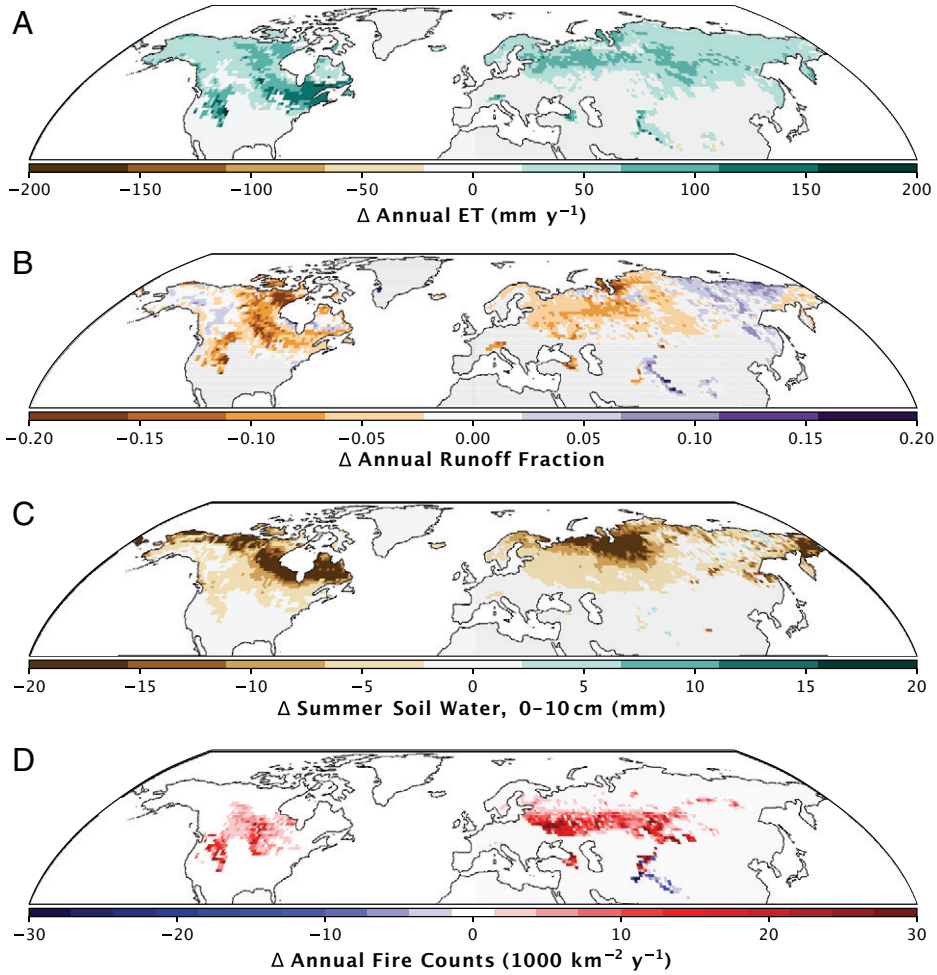

Fig. 2. Pervasive changes in ecosystem water fluxes, water storage, and disturbance simulated by the end of this century. Ensemble mean change in (*A*) annual ET, (*B*) annual runoff fraction, (*C*) summer soil-water storage (0 to 10 cm), and (*D*) annual fire counts per 1,000 km^2. Each plot shows the difference in the 40-member ensemble mean taken over the end of the simulation period (2070 to 2099) from the 40-member ensemble mean in the mid-20th century baseline period (1940 to 1969). The domain shown here includes gridcells that averaged at least 3 mo/y with SWE >30 mm but that were not snow covered for 12 mo out of the year for an ensemble mean climatology calculated over 1850 to 1880 (*Materials and Methods*).

the SSP3-7.0 scenario, relative to the historical baseline. Throughout the 21st century, snow accumulates later and melts earlier, increasing the number of snow-free days from 175 ± 17 d (ensemble mean ± 1 SD) to 257 ± 27 d at the end of this century, a mean increase of 82 snow-free days per year at this location. Finally, a greater fraction of snowmelt occurs during winter, prior to peak SWE, in the future scenario (ensemble mean ± 1 SD, 0.69 ± 0.26) compared with the historical baseline (0.11 ± 0.09). The simulated increase in the fraction of winter melt over the observational record is consistent with recent findings (6). Our simulations also demonstrate that the anthropogenic forced response on snow accumulation and melt dynamics emerges from the noise of natural variability early in the 21st century, suggesting that declines in snow-water resources may have already occurred (Figs. 3 and 4), which is also consistent with previous observation-based findings (57). Despite the CESM2-LE having higher atmospheric resolution than other LEs, it also exhibits biases in simulated trends over the historical period (*SI Appendix*, Figs. S2–S4) that may bias the time of emergence regionally (Fig. 4).

To validate the model at these gridcells, we subsampled mountain snowpack telemetry (SNOTEL) observations in the northern and central Rockies (red boxes in *SI Appendix*, Fig. S6) for sites where the accumulated maximum SWE over the historic period was within 1 SD of the CESM2 ensemble mean in each modeled gridcell (Fig. 3 and *SI Appendix*, Fig. S7 and *Materials and Methods*). Twenty-five stations (of 78 with long records) met these criteria in the northern Rockies and only four stations (of 71) met the criteria in the higher elevation central Rockies. With these subset observations, we assessed the simulated magnitude and trends in the number of snow-free days and the fraction of winter melt in the CESM2-LE. Snow-free days and the fraction of winter melt show good agreement with the CESM2-LE mean in both regions (Fig. 3 *C* and *D* and *SI Appendix*, Fig. S7 *C* and *D*). The CESM2-LE also captures observed internal variability in the system, as the width of the ensemble spread is reasonably consistent with observed year-to-year variability. Finally, consistent trends in the number of snow-free days and fraction of winter melt are evident in both the observations and CESM2-LE, especially in the northern Rockies. Although the model generally underestimates snowpack magnitude at the higher elevations where most observations are made, the agreement with observed trends, snow-free days, and winter melt lends support for simulated global-scale changes in snow and snowmelt dynamics, especially in regions without complex mountainous terrain.

Our results indicate that climate change will cause pervasive modification to snow accumulation and melt across the Northern Hemisphere. Snow cover often limits the length of the growing season in snow-dominated ecosystems (58). Across the domain, the number of snow-free days increases by 45 ± 19 d (ensemble mean ± 1 SD) by the end of the 21st century,

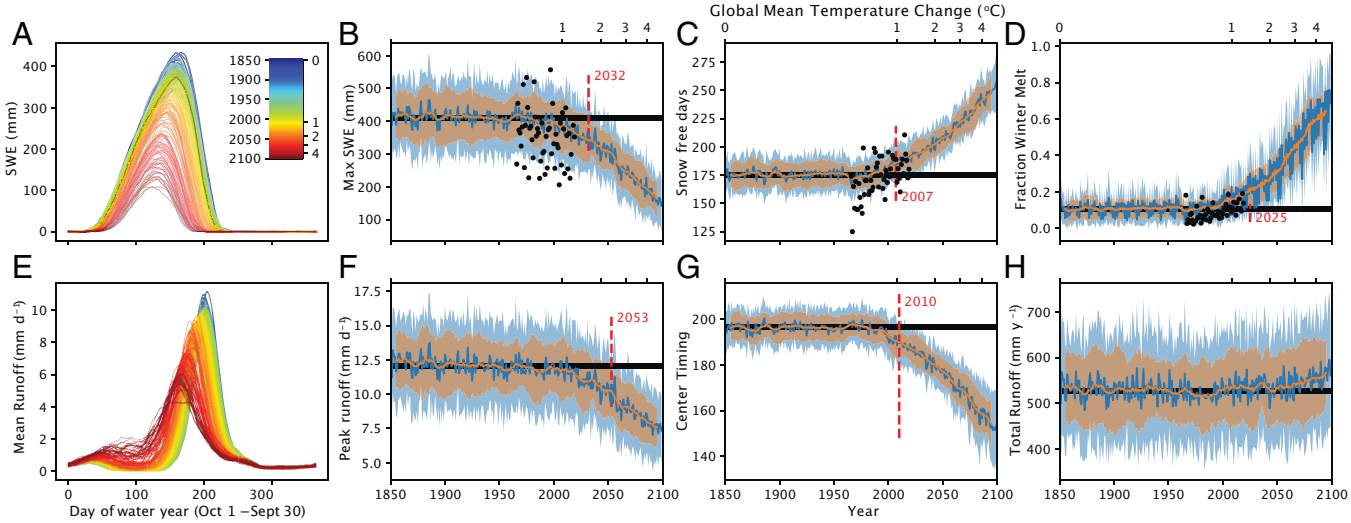

Fig. 3. Declining snowpack and increased variability in winter snowmelt and runoff. Ensemble mean annual cycle of daily (*A*) SWE and (*E*) runoff for a gridcell in the northern Rocky Mountains, United States, with line colors corresponding to simulation years and associated changes in global mean temperature. Other panels show time series and changes in global mean temperature of the ensemble mean ± 2 SD (lines and shading, respectively) for snow- and runoff-related metrics (*Upper* and *Lower* rows, respectively) including the (*B*) maximum (max) SWE (mm); (*C*) number of snow-free days per water year; (*D*) fraction of winter snow melt that occurs before peak SWE; (*F*) annual peak runoff rates (mm d^{-1}); (*G*) date of center timing (day of water year when 50% of the annual runoff has occurred); and (*H*) total water-year runoff (mm y^{-1}). The ensemble mean baseline state (1940 to 1969), annual ensemble mean, and 10-y running mean are illustrated with black, blue, and orange lines, respectively. The time of emergence is defined as the year when the baseline model state is outside of the rolling ensemble mean ± 2 SD (dashed red line). Mean annual observations for snow variables taken from a subset of SNOTEL sites in the northern Rocky Mountain region (*SI Appendix*, Fig. S6) with similar maximum SWE values are shown with black dots in the *Top* row of the figure.

relative to the historical baseline, with the largest changes occurring in temperate and coastal regions (*SI Appendix*, Fig. S8). We see an early time of emergence (*Materials and Methods*), typically before 2040, of more snow-free days across the CESM2-LE. This loss of snow cover under climate change scenarios has been reported elsewhere (59) and has important implications for the energy balance, hydrology, carbon cycle, and ecosystem function of historically snow-dominated ecosystems (1, 11, 60); but the changes are not experienced uniformly across geographic regions. For example, the mean fraction of winter snowmelt shows spatial patterns that mirror changes in the number of snow-free days, with the largest increases in relatively warmer midlatitudes and high-latitude maritime ecosystems, the latter potentially related to reductions in sea ice (Fig. 4) (4, 61). The fraction of winter melt, which is less sensitive to changes in spring snow cover than the snow-free days metric, shows an increase in ensemble variability that leads to a more heterogeneous (and later) time of emergence, as well as greater variability in runoff, particularly in winter.

Declining Predictability of Freshwater Ecosystems and Water Resources. Changes in snow accumulation and melt have impacts on aquatic ecosystems as well as the human use and management of freshwater resources. As with snow, we first illustrate these dynamics in the CESM2-LE at individual gridcells before exploring global results. With declining snowpack, the peak runoff rates simulated in both northern and central Rockies gridcells are lower, and they occur earlier in the water year (Fig. 3 and *SI Appendix*, Fig. S7, *Lower* panels). Concurrently, the center timing, or date when 50% of the annual runoff has occurred, also shifts earlier in the water year. The forced trends in the center timing of runoff emerge from the internal variability several decades earlier than changes in peak runoff in these two temperate gridcells. By the end of the 21st century, however, the internal variability in center timing increases markedly from its historical baseline (ensemble mean ± 1 SD, 196 ± 9 vs. 153 ± 15 d in baseline and future periods, respectively). Despite clear and directional changes in peak runoff rates and their timing, total water-year runoff shows little change through 2100 at this gridcell and the change does not emerge from internal variability in the model (Fig. 3*H*). Water-year runoff does not change, because runoff from winter snowmelt (defined here as runoff that occurs before peak SWE) and rain compensate for declines in peak runoff rates under the future scenario. These results illustrate that climate change can drive shifts in the mean hydrologic state but can also sustain forced changes in the seasonal cycle as well as internal variability.

Climate change decreases the predictability of pulses in spring runoff from snowmelt (Fig. 4*B*). Ecosystems and water management systems in regions like the western United States benefit from these highly predictable runoff pulses, which compose two-thirds of annual streamflow (62). The forced response of climate change results in an earlier center timing of runoff but also a dramatic increase in its variability, especially when compared with changes in variability in the number of snow-free days (Fig. 4*D* vs. *SI Appendix*, Fig. S8*B*). Together, spatial heterogeneity in the ensemble mean response and increases in ensemble variability generate high geographic variability in the time of emergence for the center timing of runoff (Fig. 4*F*). By contrast, total water-year runoff shows high spatial coherence, with declines in the continental interior and increases in maritime regions and relatively modest changes in variability (*SI Appendix*, Fig. S9). The forced response is generally weak, however, compared with internal variability in total runoff. Thus, the projected time of emergence for changes in annual mean runoff is late in the 21st century, if it occurs at all (Fig. 3*G* and *SI Appendix*, Figs. S7*G* and S9*C*).

The LE simulations also provide a means to explore the relationship between SWE and water-year runoff, which can be considered a measure of the predictability of runoff from SWE. In the baseline period (1940 to 1969), snow accumulation effectively buffers the effects of stochastic precipitation events on runoff, leading to highly predictable water-year runoff from maximum SWE and relatively low variation among ensemble members (Fig. 5*A*, blue). The loss of this snow buffer in the future scenario means that runoff quantity and timing more closely reflect the stochastic character of

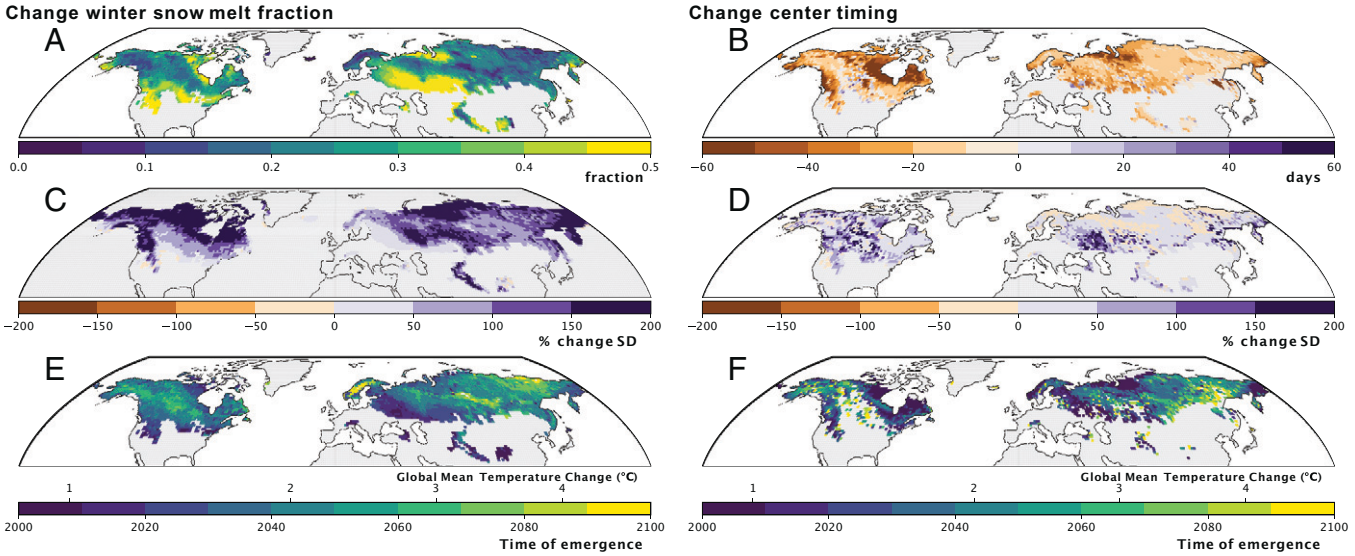

Fig. 4. Increase in the winter snowmelt fraction and earlier center timing of runoff also show increased variability. Panels show changes in the fraction of winter snowmelt that occurs before peak SWE and date of center timing of runoff (*Left* and *Right* columns, respectively), including (*A* and *B*) change in the ensemble mean state, (*C* and *D*) percent change in the ensemble SD (after removing the ensemble mean), and (*E* and *F*) the time of emergence with associated changes in global mean temperature. Changes in ensemble mean and SD were calculated as the difference across all ensemble members at the end of the 21st century (2070 through 2099) from a 30-y baseline period in the mid-20th century (1940 to 1969). As in Fig. 3, the time of emergence was calculated as the year when the 10-y running mean was ± 2 SD outside of the ensemble mean from 1940 to 1969. The color bar range in (*C* and *D*) was chosen to facilitate comparison of changes in variability between metrics. Gridcells in the domain that are not colored in (*E* and *F*) do not emerge by 2100.

precipitation. Accordingly, the correlation between SWE and runoff reduces in the future, as does the ensemble mean slope of this relationship (Fig. 5*A*, orange). This suggests a reduced predictability of runoff and drought from seasonal snowpack in the future (5).

Importantly, we see substantial increases in the variation of regression slopes between SWE and runoff. During the baseline period, any individual ensemble member approximates the ensemble mean relationship between SWE and runoff. In the future scenario, however, internal variability of the ecohydrological conditions increase under climate change. As such, a single ensemble member may show a response that ranges from no dependence of runoff on SWE, where streamflow responds to synoptic precipitation events, to a fully snow-dominated hydrologic response that is similar to the historical baseline. Thus, results from any single ensemble member may not be broadly representative of likely SWE-runoff relationships that are better captured by the ensemble mean statistics. This finding illustrates an example application of a LE to identify potential forced changes in predictability of ecosystem function, particularly over local to regional scales. However, the concept can also apply more generally.

Across the domain, maximum gridcell SWE in the CESM2-LE serves as a robust predictor for total water-year runoff over historically snow-dominated regions during the baseline period, but this predictability weakens under the future scenario ($r = 0.54 \pm 0.19$ vs. 0.41 ± 0.22, respectively ($r \pm 1$ SD); Fig. 5 *B*–*D*). Many regions that exhibited the greatest predictability of runoff–SWE relationships in the historical period experience the largest decline in predictability in the future (e.g., Rocky Mountains, Canadian Arctic, eastern North America, Eastern Europe). Thus, the largest changes in runoff predictability from SWE are in regions that historically depended on a spring pulse of runoff, further complicating the management of freshwater resources for downstream users and ecosystem health. We acknowledge that these projections may be less reliable across mountainous terrain like the Rocky Mountains, where the CESM2-LE lacks sufficient resolution to capture high altitude snow dynamics, although they qualitatively agree well with high-resolution projections (63). The extensive declines in SWE–runoff correlations in areas like eastern North America and Europe, however, suggest that natural and human systems will rely more heavily on rainfall-derived runoff and infiltration, which do not have the same predictability or temporal dependability as seasonal snowmelt–driven pulses of water to soils and streams.

Our findings highlight the pervasive forced changes to the mean state and variability of snow accumulation, snow melt, and runoff that may be expected in historically snow-dominated regions. In model projections, reduced SWE accumulation and earlier snowmelt timing result in an increase in the number of snow-free days that will potentially extend the growing season over much of the Northern Hemisphere, resulting in drier soils and increased fire risk. Changes to snow hydrology also drive increased variability in the timing of runoff and a decrease in the predictability of annual runoff from maximum SWE. Collectively, these alterations to ecohydrological function present compound challenges to developing adaptation and mitigation strategies that can meet pressures from forced changes in the hydrological cycle.

Materials and Methods

CESM2 LE. The simulations used here are from the 100-member LE suite with CESM2 (37), namely the CESM2-LE (26). The simulations are conducted over the years 1850 to 2100, following CMIP6 protocols for historical and SSP3-7.0 forcing (64). The choice of the relatively high-emissions pathway SSP3-7.0 follows the suggestions of the CMIP6 protocols for LE simulations (65). The CAM6 atmospheric component of the model has a horizontal resolution of 1.25° in longitude and 0.9° in latitude, with 32 levels in the vertical and a top at 2.26 hPa.

The CESM2-LE offers two significant advantages over other available LEs for the specific research questions pursued in this study. First, enhancements available with the terrestrial component of CESM2, the CLM5 land model, provide improved process representation of both hydrological processes and biogeochemistry (40, 54, 66–69). Detailed documentation of the improved skill in CLM5 has been identified through evaluation of the model with the International Land Model Benchmarking (ILAMB; version 2.1) diagnostics (40, 70).

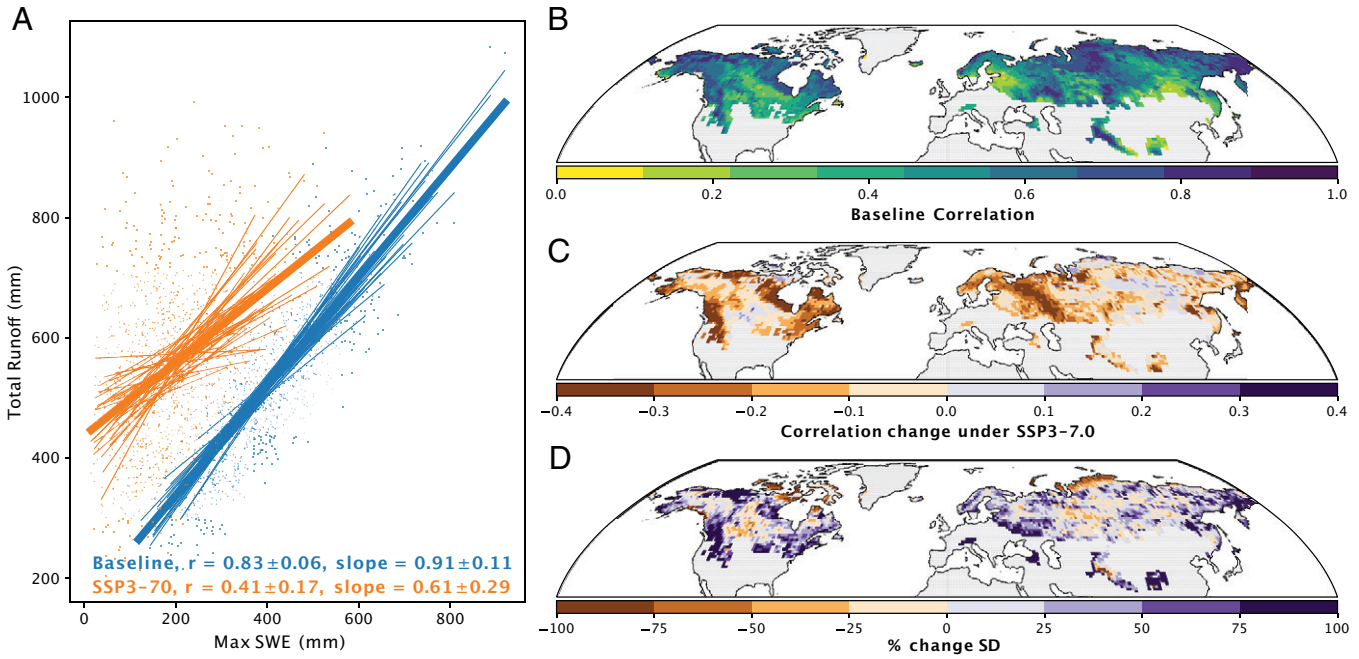

Fig. 5. Declining predictability of annual runoff from SWE. Panels show the (*A*) relationships between maximum (max) annual SWE (mm) and total water-year runoff (mm) for each ensemble member in the northern Rocky Mountains of the United States; (*B*) the mean ensemble correlation between SWE runoff across the historically snow-covered domain during the baseline period (1940 to 1969); (*C*) reductions in the predictability between SWE and runoff in future scenarios (2070 through 2099); and (*D*) changes in the normalized SD of the linear slope of the maximum SWE: total runoff relationships in the future scenario vs. the baseline period. (*A*) Thin lines show linear correlations between SWE and runoff from individual ensemble members between 1940 and 1969 and 2070 and 2099 (blue and orange lines, respectively). Thick lines show the ensemble mean, thin lines show individual ensemble members, dots show individual years. The correlation (*r*) and regression slopes (mean ± 1 SD) taken across 40 ensemble members) for the baseline and future periods are provided.

More broadly, the skill of CESM2 has been extensively demonstrated, with the model performing well for various skill metrics relative to other models (38, 39). Second, and equally important, is the resolution of CAM6 as the atmospheric component of CESM2, which is higher than many other LEs that represent both land hydrological and biogeochemical processes [e.g., CanESM5 (71) with 2.8°×°2.8 resolution in the atmosphere, and the model from the Max Planck Institute (72) with effective 1.8°×°1.8 resolution]. It, therefore, offers reduced smoothing of orographic features that are known to impact hydrology and the mean climate state. Despite these improvements, we acknowledge that the nominal 1-degree resolution of the CESM2-LE still presents a spatial mismatch when trying to compare simulations to local observations of snow depth and runoff, especially in topographically complex terrain (discussed in *Materials and Methods*). Aside from these more scientific advantages offered through improved process representation, as a practical matter, extensive high-frequency (daily mean) model output was saved for ensemble members of CESM2-LE, allowing for resolution of details of forced changes in the seasonal cycle.

CESM2 LE Analyses. The analyses presented here use 40 members from the CESM2-LE, which saved high-frequency output and used the default biomass burning inputs to the atmosphere that were defined in the CMIP6 protocol (26). We have not evaluated the ensemble members that used smoothed biomass-burning emissions during the satellite era. First, we defined the domain of historically snow-dominated regions as gridcells in the Northern Hemisphere where the ensemble mean monthly SWE over the initial years of the simulation (1850 to 1880) was greater than 30 mm for at least 3 mo of the year. We also excluded terrestrial gridcells that were initially snow covered for 12 mo of the year from our analysis. Second, to characterize changes in the mean state, we looked at a climatology of monthly results under the ensemble mean baseline state (1940 to 1969) and future scenario (2070 to 2099).

Preliminary analyses suggested that baseline seasonal cycle (Fig. 1) and time of emergence (Fig. 4) are relatively insensitive to the choice of years used for this baseline period, given the relatively stable ensemble mean for the first century of the historic period (e.g., Fig. 3). The baseline period used here was chosen to pick a period that was chronologically closer to the observational record. We quantified changes in the domain mean state (weighted by gridcell area; e.g., Fig. 1) and over individual gridcells for several metrics, including precipitation, temperature, SWE, GPP, runoff, soil water (0 to 10 cm), soil-moisture stress, ET, and fire counts. Fire counts in CLM5 are calculated prognostically as the product of ignition sources (from lightning strikes and human sources), the availability of fuels, the combustibility of fuel (calculated as a function of relative humidity, soil moisture, and soil temperature), and anthropogenic suppression of fire occurrence (40). The annual runoff and ET fraction are calculated as the ratio of the respective annual fluxes to the annual precipitation (Fig. 2 and *SI Appendix*, Fig. S5).

To investigate changes in the mean state and variance related to snow accumulation, snowmelt, and runoff, we used daily data of SWE and runoff from the same 40 ensemble members of the CESM2-LE. We assessed water years (October 1 through September 30) over the simulation period (water years beginning in 1850 to 2099). To reduce the dimensionality of these data, we identified several metrics to quantify changes in the ensemble mean state and ensemble variability. For SWE, these included maximum water-year SWE, the number of snow-free days, and the fraction of winter melt, here defined as the amount of melt occurring before peak SWE (6). For runoff, these included peak discharge, center timing of runoff (the day when 50% of the annual water year runoff occurred), and total water-year runoff (Fig. 3 and *SI Appendix*, Fig. S7).

At each gridcell, we calculated the ensemble mean and SD for these metrics across all water years. We also smoothed results by taking a centered 10-y rolling mean for each ensemble member and then calculating ensemble statistics. We defined the time of emergence as the water year when the running ensemble mean ± 2 SD was outside the ensemble mean from the baseline period (1940 to 1969). To facilitate comparisons with other LEs, we also provide, besides time of emergence, the associated temperature of emergence, which corresponds to the changes in global mean temperature that are simulated by the 40-member CESM2-LE at the time of emergence.

We report normalized changes in ensemble variability by calculating the difference in ensemble variability at the end of this century (calculated between 2070 and 2099) from its baseline period and divided by the baseline variability (Fig. 4 and *SI Appendix*, Figs. S8 and S9). Finally, to look at predictability of SWE–runoff relationships, we calculated Pearson's correlation coefficients for individual ensemble members over the 30 y of each baseline period and future

scenario (Fig. 5*A*). We also report the ensemble mean statistics of these correlations across the domain during the baseline period and their change by the end of this century (Fig. 5 *B*–*D*).

Observational Comparisons. We compared ensemble mean results with observational benchmarks provided with the ILAMB model benchmarking package, which are commonly used to evaluate land model output (40, 70). For individual metrics, ILAMB includes several benchmarking datasets, but to simplify our analysis, we used observation-based datasets of air temperature from the Climatic Research Unit (which covers 1979 to 2012) (73); precipitation from GPCP2 (covering 1979 to 2012) (74); SWE globally (covering 1981 to 2010) (1) and over the conterminous United States (not part of ILAMB covering 1982 to 2020) (49); GPP from Fluxnet-MTE (covering 1982 to 2008) (75); runoff from Linear Optimal Runoff Aggregate (covering 1980 to 2012) (76); and ET from the Global Land surface Evaporation: the Amsterdam Methodology (covering 1980 to 2018) (77). Observational data were regridded to the nominal 1-degree resolution of the CESM2-LE, averaged across years, and weighed by land area to produce monthly climatologies shown in Fig. 1. The monthly climatology from CESM2-LE results from the baseline period (1940 to 1969 and shown in Fig. 1) were not significantly different from the later period (1970 to 2020) that better overlaps with the observation-based datasets.

Using these same observation-based datasets, we calculated spatial biases in the ensemble mean state and trends (*SI Appendix*, Figs. S1–S4). For these analyses, CESM2-LE statistics were calculated over the period from 1970 to 2020. Spatial biases in the CESM2-LE were calculated by subtracting the ensemble mean climatology from the observed historical climatology at each gridcell (*SI Appendix*, Fig. S1). Given our focus on snow, biases and trends in temperature and precipitation were only calculated over winter months (October to March), for water-year maximum SWE (from monthly data in global comparisons and daily data over the conterminous United States to match temporal resolution of SWE for observational datasets) and the annual sum of other variables. Gridcell linear trends over the historical record for winter temperature, winter precipitation, and maximum SWE were calculated for each CEMS2-LE member and for each observation-based dataset (*SI Appendix*, Figs. S2–S4). We report ensemble mean trends and their bias from observational trends. We then ranked the trends reported in observations within the spread of the ensemble members to evaluate if the CESM2-LE spread encompasses the direction and magnitude of observed trends in temperature, precipitation, and maximum SWE over the historical record.

While the mountain snowpack of the US Rocky Mountains is closely monitored with a network of remote telemetry stations with 30- to >40-y SNOTEL records, the coarse spatial resolution of climate models, contrasted with the complex terrain where the snowpack monitoring stations are located, generally precludes a direct comparison (78, 79). Compared with neighboring lower elevations, high-elevation catchments can act as water towers (60) that disproportionately contribute more snowmelt runoff due to colder and wetter climate regimes. For example, 44% ($n = 34$ of 78 stations) and 100% ($n = 71$) of regional snowpack monitoring stations with long records are located higher in elevation than the mean elevation of the "snowiest" CESM2 pixel centered on the northern and central Rocky Mountains, respectively (Fig. 3 and *SI Appendix*, Figs. S6 and S7). Acknowledging the elevation discrepancy and inability of the model to represent the region's most substantial mountain snow-water resources, we subsampled SNOTEL observations in the northern and central Rockies regions for sites where long-term mean maximum annual SWE over the historic period was within 1 SD of the CESM2 ensemble mean for selected gridcells. We show the annual mean across observational sites meeting these criteria in Fig. 3 and *SI Appendix*, Fig. S7.

Data Availability. Previously published data were used for this work: https://www.earthsystemgrid.org/dataset/ucar.cgd.cesm2le.output.html. CESM2-LENS data are available from the National Center for Atmospheric Research's Climate Data Gateway (https://www.earthsystemgrid.org/dataset/ucar.cgd.cesm2le.output.html). The notebooks used for the analysis and graphics in this article are available from GitHub at https://github.com/wwieder/CESM2-LE_SnowWater; and code used for analysis and display items are available on Zenodo at https://zenodo.org/record/6585398#.Ypo5rHbMLcs.

ACKNOWLEDGMENTS. The simulations presented here were coordinated and conducted by Sun-Seon Lee at the Institute for Basic Sciences Center for Climate Physics (ICCP) and Jim Edwards at the National Center for Atmospheric Research (NCAR) on the Institute for Basic Sciences (IBS/ICCP supercomputer "Aleph," a high-performance Cray XC50-E Skylake computing system. The CESM project is supported primarily by the NSF. This material is based upon work supported by NCAR, which is a major facility sponsored by the NSF under Cooperative Agreement No. 1852977. Computing and data storage resources, including the Cheyenne supercomputer (doi:10.5065/D6RX99HX), were provided by the Computational and Information Systems Laboratory at NCAR. We thank all the scientists, software engineers, and administrators who contributed to the development of CESM2. W.R.W. also acknowledges support from the NSF (Awards 2031238, 2120804, and 1637686). The work of K.B.R. and R.Y. were supported by Institute for Basic Science (IBS), Republic of Korea, Grant IBS-R028-D1. F.L. and N.R. are supported by the U.S. Department of Energy, Office of Science, Office of Biological & Environmental Research (BER), Regional and Global Model Analysis (RGMA) component of the Earth and Environmental System Modeling Program under Award Number DE-SC0022070 through the NSF interagency agreeement 1947282. F.L. is also suppored by the National Oceanic and Atmospheric Administration (NOAA) award 4310349.

Author affiliations: [a]Climate and Global Dynamics Laboratory, National Center for Atmospheric Research, Boulder, CO 80307; [b]Institute of Arctic and Alpine Research, University of Colorado Boulder, Boulder, CO 80309; [c]Department of Earth and Atmospheric Sciences, Cornell University, Ithaca, NY 14853; [d]Center for Climate Physics, Institute for Basic Science, Busan 46241, South Korea; and [e]Pusan National University, Busan 46241, South Korea

1. L. Mudryk *et al.*, Historical Northern Hemisphere snow cover trends and projected changes in the CMIP6 multi-model ensemble. *Cryosphere* **14**, 2495–2514 (2020).
2. T. P. Barnett, J. C. Adam, D. P. Lettenmaier, Potential impacts of a warming climate on water availability in snow-dominated regions. *Nature* **438**, 303–309 (2005).
3. T. P. Barnett *et al.*, Human-induced changes in the hydrology of the western United States. *Science* **319**, 1080–1083 (2008).
4. F. Lehner *et al.*, Mitigating the impacts of climate nonstationarity on seasonal streamflow predictability in the U.S. southwest. *Geophys. Res. Lett.* **44**, 12208–12217 (2017).
5. B. Livneh, A. M. Badger, Drought less predictable under declining future snowpack. *Nat. Clim. Chang.* **10**, 452–458 (2020).
6. K. N. Musselman, N. Addor, J. A. Vano, N. P. Molotch, Winter melt trends portend widespread declines in snow water resources. *Nat. Clim. Chang.* **2021**, 418–424 (2021).
7. I. T. Stewart, D. R. Cayan, M. D. Dettinger, Changes toward earlier streamflow timing across western North America. *J. Clim.* **18**, 1136–1155 (2005).
8. V. H. Dale *et al.*, Climate change and forest disturbances. *Bioscience* **51**, 723–734 (2001).
9. J. S. Mankin, R. Seager, J. E. Smerdon, B. I. Cook, A. P. Williams, Mid-latitude freshwater availability reduced by projected vegetation responses to climate change. *Nat. Geosci.* **12**, 983–988 (2019).
10. A. L. Swann, F. M. Hoffman, C. D. Koven, J. T. Randerson, Plant responses to increasing CO_2 reduce estimates of climate impacts on drought severity. *Proc. Natl. Acad. Sci. U.S.A.* **113**, 10019–10024 (2016).
11. D. R. Cayan, M. D. Dettinger, S. A. Kammerdiener, J. M. Caprio, D. H. Peterson, Changes in the onset of spring in the western United States. *Bull. Am. Meteorol. Soc.* **82**, 399–415 (2001).
12. G. J. McCabe, J. L. Betancourt, G. T. Pederson, M. D. Schwartz, Variability common to first leaf dates and snowpack in the western conterminous United States. *Earth Interact.* **17**, 1–18 (2013).
13. T. R. Ault, M. D. Schwartz, R. Zurita-Milla, J. F. Weltzin, J. L. Betancourt, Trends and natural variability of spring onset in the coterminous United States as evaluated by a new gridded dataset of spring indices. *J. Clim.* **28**, 8363–8378 (2015).
14. S.-J. Jeong, C.-H. Ho, H.-J. Gim, M. E. Brown, Phenology shifts at start vs. end of growing season in temperate vegetation over the Northern Hemisphere for the period 1982-2008. *Glob. Change Biol.* **17**, 2385–2399 (2011).
15. T. F. Keenan *et al.*, Net carbon uptake has increased through warming-induced changes in temperate forest phenology. *Nat. Clim. Chang.* **4**, 598–604 (2014).
16. Z. Zhu *et al.*, Greening of the Earth and its drivers. *Nat. Clim. Chang.* **6**, 791–795 (2016).
17. I. H. Myers-Smith *et al.*, Complexity revealed in the greening of the Arctic. *Nat. Clim. Chang.* **10**, 106–117 (2020).
18. W. Buermann *et al.*, Widespread seasonal compensation effects of spring warming on northern plant productivity. *Nature* **562**, 110–114 (2018).
19. W. Buermann, P. R. Bikash, M. Jung, D. H. Burn, M. Reichstein, Earlier springs decrease peak summer productivity in North American boreal forests. *Environ. Res. Lett.* **8**, 024027 (2013).
20. A. L. Westerling, Increasing western US forest wildfire activity: Sensitivity to changes in the timing of spring. *Philos. Trans. R. Soc. Lond. B Biol. Sci.* **371**, 20150178 (2016).
21. A. L. Westerling, H. G. Hidalgo, D. R. Cayan, T. W. Swetnam, Warming and earlier spring increase western U.S. forest wildfire activity. *Science* **313**, 940–943 (2006).
22. P. J. CaraDonna, A. M. Iler, D. W. Inouye, Shifts in flowering phenology reshape a subalpine plant community. *Proc. Natl. Acad. Sci. U.S.A.* **111**, 4916–4921 (2014).
23. D. W. Inouye, Effects of climate change on phenology, frost damage, and floral abundance of montane wildflowers. *Ecology* **89**, 353–362 (2008).
24. F. Lehner *et al.*, Partitioning climate projection uncertainty with multiple large ensembles and CMIP5/6. *Earth Syst. Dyn.* **11**, 491–508 (2020).

25. A. G. Pendergrass, R. Knutti, F. Lehner, C. Deser, B. M. Sanderson, Precipitation variability increases in a warmer climate. *Sci. Rep.* **7**, 17966 (2017).
26. K. B. Rodgers *et al.*, Ubiquity of human-induced changes in climate variability. *Earth Syst. Dynam. Discuss.* **2021**, 1–22 (2021).
27. R. W. Katz, B. G. Brown, Extreme events in a changing climate: Variability is more important than averages. *Clim. Change* **21**, 289–302 (1992).
28. G. A. Meehl *et al.*, An introduction to trends in extreme weather and climate events: Observations, socioeconomic impacts, terrestrial ecological impacts, and model projections. *Bull. Am. Meteorol. Soc.* **81**, 413–416 (2000).
29. D. R. Easterling *et al.*, Climate extremes: Observations, modeling, and impacts. *Science* **289**, 2068–2074 (2000).
30. G. Branstator, F. Selten, "Modes of variability" and climate change. *J. Clim.* **22**, 2639–2658 (2009).
31. C. Deser *et al.*, Insights from Earth system model initial-condition large ensembles and future prospects. *Nat. Clim. Chang.* **10**, 277–286 (2020).
32. H. Zelle, G. Jan van Oldenborgh, G. Burgers, H. Dijkstra, El Niño and greenhouse warming: Results from ensemble simulations with the NCAR CCSM. *J. Clim.* **18**, 4669–4683 (2005).
33. D. Lombardozzi, G. B. Bonan, D. W. Nychka, The emerging anthropogenic signal in land-atmosphere carbon-cycle coupling. *Nat. Clim. Chang.* **4**, 796–800 (2014).
34. N. S. Lovenduski, G. B. Bonan, Reducing uncertainty in projections of terrestrial carbon uptake. *Environ. Res. Lett.* **12**, 044020 (2017).
35. J. S. Mankin *et al.*, Blue water trade-offs with vegetation in a CO_2-enriched climate. *Geophys. Res. Lett.* **45**, 3115–3125 (2018).
36. D. Touma, S. Stevenson, F. Lehner, S. Coats, Human-driven greenhouse gas and aerosol emissions cause distinct regional impacts on extreme fire weather. *Nat. Commun.* **12**, 212 (2021).
37. G. Danabasoglu *et al.*, The Community Earth System Model version 2 (CESM2). *J. Adv. Model. Earth Syst.* **12**, e2019MS001916 (2020).
38. J. T. Fasullo, Evaluating simulated climate patterns from the CMIP archives using satellite and reanalysis datasets using the Climate Model Assessment Tool (CMATv1). *Geosci. Model Dev.* **13**, 3627–3642 (2020).
39. J. T. Fasullo, A. S. Phillips, C. Deser, Evaluation of leading modes of climate variability in the CMIP archives. *J. Clim.* **33**, 5527–5545 (2020).
40. D. M. Lawrence *et al.*, The Community Land Model version 5: Description of new features, benchmarking, and impact of forcing uncertainty. *J. Adv. Model. Earth Syst.* **11**, 4245–4287 (2019).
41. I. R. Simpson *et al.*, An evaluation of the large-scale atmospheric circulation and its variability in CESM2 and other CMIP models. *J. Geophys. Res. Atmos.* **125**, e2020JD032835 (2020).
42. K. Kouki, P. Räisänen, K. Luojus, A. Luomaranta, A. Riihelä, Evaluation of Northern Hemisphere snow water equivalent in CMIP6 models during 1982–2014. *Cryosphere* **16**, 1007–1030 (2022).
43. S. Swenson, Assessing high-latitude winter precipitation from global precipitation analyses using GRACE. *J. Hydrometeorol.* **11**, 405–420 (2010).
44. P. D. Broxton, X. Zeng, N. Dawson, Why do global reanalyses and land data assimilation products underestimate snow water equivalent? *J. Hydrometeorol.* **17**, 2743–2761 (2016).
45. L. R. Mudryk, C. Derksen, P. J. Kushner, R. Brown, Characterization of Northern Hemisphere snow water equivalent datasets, 1981–2010. *J. Clim.* **28**, 8037–8051 (2015).
46. X. Zeng, P. Broxton, N. Dawson, Snowpack change from 1982 to 2016 over conterminous United States. *Geophys. Res. Lett.* **45**, 12940–12947 (2018).
47. E. Cho, J. M. Jacobs, C. M. Vuyovich, The value of long-term (40 years) airborne gamma radiation SWE record for evaluating three observation-based gridded SWE data sets by seasonal snow and land cover classifications. *Water Resour. Res.* **56**, e2019WR025813 (2020).
48. M. Girotto, K. N. Musselman, R. L. H. Essery, Data assimilation improves estimates of climate-sensitive seasonal snow. *Curr. Clim. Change Rep.* **6**, 81–94 (2020).
49. P. Broxton, X. Zeng, N. Dawson, Daily 4 km gridded SWE and snow depth from assimilated in-situ and modeled data over the conterminous US, Version 1. NASA National Snow and Ice Data Center Distributed Active Archive Center. https://nsidc.org/data/NSIDC-0719/versions/1. Accessed 4 January 2022.
50. M. A. Brunke, J. Welty, X. Zeng, Attribution of snowpack errors to simulated temperature and precipitation in E3SMv1 over the contiguous United States. *J. Adv. Model. Earth Syst.* **13**, e2021MS002640 (2021).
51. J. Liu, P. O. Wennberg, N. C. Parazoo, Y. Yin, C. Frankenberg, Observational constraints on the response of high-latitude northern forests to warming. *AGU Advances.* **1**, e2020AV000228 (2020).
52. B. Zhou, P. Zhai, Y. Chen, R. Yu, Projected changes of thermal growing season over Northern Eurasia in a 1.5 °C and 2 °C warming world. *Environ. Res. Lett.* **13**, 035004 (2018).
53. Z. Butterfield, W. Buermann, G. Keppel-Aleks, Satellite observations reveal seasonal redistribution of northern ecosystem productivity in response to interannual climate variability. *Remote Sens. Environ.* **242**, 111755 (2020).
54. W. R. Wieder, Z. Butterfield, K. Lindsay, D. L. Lombardozzi, G. Keppel-Aleks, Interannual and seasonal drivers of carbon cycle variability represented by the Community Earth System Model (CESM2). *Global Biogeochemical Cycles* **35**, e2021GB007034 (2021).
55. B. M. Sanderson, R. A. Fisher, A fiery wake-up call for climate science. *Nat. Clim. Chang.* **10**, 175–177 (2020).
56. B. M. Rogers, J. K. Balch, S. J. Goetz, C. E. R. Lehmann, M. Turetsky, Focus on changing fire regimes: Interactions with climate, ecosystems, and society. *Environ. Res. Lett.* **15**, 030201 (2020).
57. P. W. Mote, S. Li, D. P. Lettenmaier, M. Xiao, R. Engel, Dramatic declines in snowpack in the western US. *npj Clim. Atmos. Sci.* **1**, 2 (2018).
58. D. S. Grogan, E. A. Burakowski, A. R. Contosta, Snowmelt control on spring hydrology declines as the vernal window lengthens. *Environ. Res. Lett.* **15**, 114040 (2020).
59. L. R. Mudryk, P. J. Kushner, C. Derksen, C. Thackeray, Snow cover response to temperature in observational and climate model ensembles. *Geophys. Res. Lett.* **44**, 919–926 (2017).
60. W. W. Immerzeel *et al.*, Importance and vulnerability of the world's water towers. *Nature* **577**, 364–369 (2020).
61. C. Deser, L. Terray, A. S. Phillips, Forced and internal components of winter air temperature trends over North America during the past 50 years: Mechanisms and implications. *J. Clim.* **29**, 2237–2258 (2016).
62. D. Li, M. L. Wrzesien, M. Durand, J. Adam, D. P. Lettenmaier, How much runoff originates as snow in the western United States, and how will that change in the future? *Geophys. Res. Lett.* **44**, 6163–6172 (2017).
63. K. Ikeda *et al.*, Snowfall and snowpack in the Western U.S. as captured by convection permitting climate simulations: Current climate and pseudo global warming future climate. *Clim. Dyn.* **57**, 2191–2215 (2021).
64. V. Eyring *et al.*, Overview of the Coupled Model Intercomparison Project Phase 6 (CMIP6) experimental design and organization. *Geosci. Model Dev.* **9**, 1937–1958 (2016).
65. B. C. O'Neill *et al.*, The Scenario Model Intercomparison Project (ScenarioMIP) for CMIP6. *Geosci. Model Dev.* **9**, 3461–3482 (2016).
66. G. B. Bonan *et al.*, Model structure and climate data uncertainty in historical simulations of the terrestrial carbon cycle (1850–2014). *Global Biogeochem. Cycles* **33**, 1310–1326 (2019).
67. D. Kennedy *et al.*, Implementing plant hydraulics in the Community Land Model, version 5. *J. Adv. Model. Earth Syst.* **11**, 485–513 (2019).
68. D. L. Lombardozzi *et al.*, Simulating agriculture in the Community Land Model version 5. *J. Geophys. Res. Biogeo.* **125**, e2019JG005529 (2020).
69. W. R. Wieder *et al.*, Beyond static benchmarking: Using experimental manipulations to evaluate land model assumptions. *Global Biogeochem. Cycles* **33**, 1289–1309 (2019).
70. N. Collier *et al.*, The international land model benchmarking (ILAMB) system: Design, theory, and implementation. *J. Adv. Model. Earth Syst.* **10**, 2731–2754 (2018).
71. N. C. Swart *et al.*, The Canadian Earth System Model version 5 (CanESM5.0.3). *Geosci. Model Dev.* **12**, 4823–4873 (2019).
72. N. Maher *et al.*, The Max Planck Institute grand ensemble: Enabling the exploration of climate system variability. *J. Adv. Model. Earth Syst.* **11**, 2050–2069 (2019).
73. I. Harris, P. D. Jones, T. J. Osborn, D. H. Lister, Updated high-resolution grids of monthly climatic observations – The CRU TS3.10 Dataset. *Int. J. Climatol.* **34**, 623–642 (2014).
74. R. F. Adler, G. Gu, G. J. Huffman, Estimating climatological bias errors for the global precipitation climatology project (GPCP). *J. Appl. Meteorol. Climatol.* **51**, 84–99 (2012).
75. G. Lasslop *et al.*, Separation of net ecosystem exchange into assimilation and respiration using a light response curve approach: Critical issues and global evaluation. *Glob. Change Biol.* **16**, 187–208 (2010).
76. S. Hobeichi, G. Abramowitz, J. Evans, H. E. Beck, Linear optimal runoff aggregate (LORA): A global gridded synthesis runoff product. *Hydrol. Earth Syst. Sci.* **23**, 851–870 (2019).
77. D. G. Miralles *et al.*, Global land-surface evaporation estimated from satellite-based observations. *Hydrol. Earth Syst. Sci.* **15**, 453–469 (2011).
78. E. D. Gutmann *et al.*, A comparison of statistical and dynamical downscaling of winter precipitation over complex terrain. *J. Clim.* **25**, 262–281 (2012).
79. F. Lehner *et al.*, The potential to reduce uncertainty in regional runoff projections from climate models. *Nat. Clim. Chang.* **9**, 926–933 (2019).